Continuum Micromechanical modeling for Interfacial Debonding of TiN/AA8090 Alloy Particulate Composites

[1]P. M. Jebaraj and A. Chennakesava Reddy[2]

[1]Professor, Department of Mechanical Engineering, Dr. Ambedkar Institute of Technology, Bangalore, India.
[2]Assistant Professor, Department of Mechanical Engineering, MJ College of Engineering and Technology, Hyderabad, India
dr_acreddy@yahoo.com

Abstract: *A square array unit cell/rhombus* TiN *nanoparticle RVE models were used to predict micromechanical behavior and interfacial debonding in AA8090/* TiN *composites. The AA8090/* TiN *particulate metal matrix composites were fabricated at three different volume fractions of* TiN*. The stiffness of the composite has increased with increase of* TiN *volume fraction. The interfacial debonding was observed in the composites.*

Keywords: AA8090*, titanium nitride, ellipsoidal nanoparticle, RVE model, finite element analysis, debonding.*

1. INTRODUCTION

Many composite materials have high particle volume fraction, such as metal matrix composite materials reinforced with 30–50% of ceramic particles to improve stiffness and wear resistance. These composite materials have high specific surface (i.e., high interface area per unit volume of the composite material) such that the behavior of particle/matrix interfaces may significantly influence the macroscopic behavior of composite materials. The interfacial debonding between matrix and particles is a major damage mechanism that governs nonlinear and anisotropic behavior of the composite material [1]. The interfacial debonding also governs fracture of composite materials with high particle volume fraction. The direct consequence of interfacial debonding is the decrease of modulus of the composite material as compared to that with perfect interfacial bonding. Another consequence of the interfacial debonding is the particle size effect, which has been repeatedly observed in composite materials with high particle volume fraction [2-17].

Titanium nitride (TiN) oxidizes at 800 °C at normal atmosphere. It is chemically stable at room temperature and is attacked by hot concentrated acids. A well-known use for TiN is for edge retention and corrosion resistance on machine tooling, such as drill bits and milling cutters, often improving their lifetime by a factor of three or more. TiN is classified as a 'barrier metal', even though it is clearly a ceramic from the perspective of chemistry or mechanical behavior. In the current work, AA8090 alloy/TiN nanoparticle composites were analyzed for interfacial debonding using RVE model through finite element analysis. Shape of the reinforced particle considered in this work is a rhombus. The periodic particle distribution was a square array as shown in figure 1.

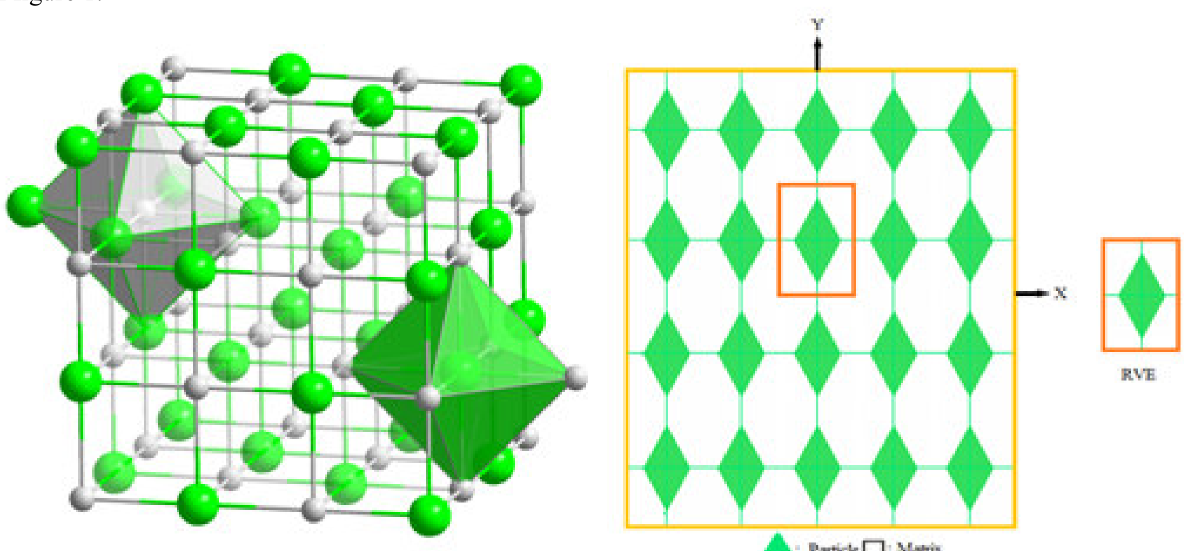

Figure 1: A diamond RVE containing a rhombus nanoparticle.

2. THEORETICAL BACKGROUND

The strains along x- and y-directions can be determined as using the following equations:

$$\varepsilon_y = -\left(\frac{v_{xy}}{E_x} + \frac{1}{E_z}\right) P = \frac{\Delta y}{a} \quad (1)$$

$$\varepsilon_x = \left(\frac{1}{E_x} - \frac{1}{E_z}\right) P = \frac{\Delta x}{a} \quad (2)$$

The effective elastic moduli and Poisson's ratio in the transverse direction (xy-plane) as follows:

$$E_x = \frac{1}{\frac{\Delta x}{Pa}+\frac{1}{E_z}} \text{ and } E_y = \frac{1}{\frac{\Delta y}{Pa}+\frac{1}{E_z}} \quad (3)$$

$$v_{xy} = \left(\frac{\Delta y}{Pa} + \frac{1}{E_z}\right) / \left(\frac{\Delta x}{Pa} + \frac{1}{E_z}\right) \quad (4)$$

Once the change in lengths along x- and y- direction (Δx and Δy) are determined for the square RVE from the FEA, E_y and E_x and v_{xy} can be determined from Eqs. (3) and (4), correspondingly. Considering adhesion, formation of precipitates, particle size, agglomeration, voids/porosity, obstacles to the dislocation, and the interfacial reaction of the particle/matrix, the formula for the strength of composite is stated below:

$$\sigma_c = \left[\sigma_m \left\{\frac{1-(v_p+v_v)^{2/3}}{1-1.5(v_p+v_v)}\right\}\right] e^{m_p(v_p+v_v)} + k d_p^{-1/2} \quad (5)$$

$$k = E_m m_m / E_p m_p$$

where, v_v and v_p are the volume fractions of voids/porosity and nanoparticles in the composite respectively, m_p and m_m are the possion's ratios of the nanoparticles and matrix respectively, d_p is the mean nanoparticle size (diameter) and E_m and E_p is elastic moduli of the matrix and the particle respectively. Elastic modulus (Young's modulus) is a measure of the stiffness of a material and is a quantity used to characterize materials. Elastic modulus is the same in all orientations for isotropic materials. Anisotropy can be seen in many composites.

The upper-bound equation is given by

$$\frac{E_c}{E_m} = \left(\frac{1-{v_v}^{2/3}}{1-{v_v}^{2/3}+v_v}\right) + \frac{1+(\delta-1){v_p}^{2/3}}{1+(\delta-1)({v_p}^{2/3}-v_p)} \quad (6)$$

The lower-bound equation is given by

$$\frac{E_c}{E_m} = 1 + \frac{v_p-v_p}{\delta/(\delta-1)-(v_p+v_v)^{1/3}} \quad (7)$$

where, $\delta = E_p / E_m$.

The transverse modulus is given by

$$E_t = \frac{E_m E_p}{E_m + E_p(1-{v_p}^{2/3})/{v_p}^{2/3}} + E_m\left(1 - {v_p}^{2/3} - {v_v}^{2/3}\right) \quad (8)$$

3. MATERIALS METHODS

The matrix material was AA8090 alloy. The reinforcement material was ellipsoidal TiN nanoparticles of average size 100nm. The mechanical properties of materials used in the present work are given in table 1.

Table 1: Mechanical properties of AA8090 matrix and TiN nanoparticles

Property	AA8090	TiN
Density, g/cc	2.54	5.22
Elastic modulus, GPa	77	251
Ultimate tensile strength, MPa	440	-
Poisson's ratio	0.33	0.25

AA8090 alloy/TiN composites were manufactured by the stir casting process and low pressure casting technique with argon gas at 3.0 bar. The composite samples were give solution treatment and cold rolled to the predefined size of tensile specimens. The heat-treated samples were machined to get flat-rectangular specimens (figure 2) for the tensile tests. The tensile specimens were placed in the grips of a Universal Test Machine (UTM) at a specified grip separation and pulled until failure. The test speed was 2 mm/min (as for ASTM D3039). A strain gauge was used to determine elongation.

In this research, a cubical representative volume element (RVE) was implemented to analyze the tensile behavior AA8090/TiN nanoparticle composites at three (10%, 20% and 30%) volume fractions of TiN. The large strain PLANE183 element was used in the matrix in all the models. In order to model the adhesion between the matrix and the particle, a CONTACT 172 element was used.

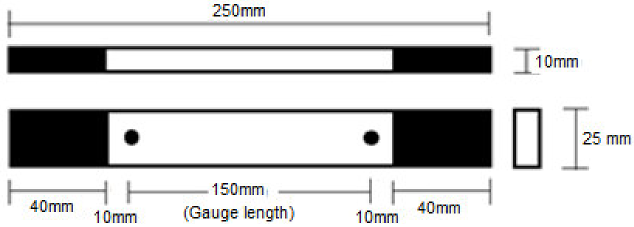

Figure 2: Shape and dimensions of tensile specimen

4. RESULTS AND DISCUSSION

The morphology of TiN particles is shown in figure 3. The crystal structure is cubic (cF8) with octahedral coordination geometry.

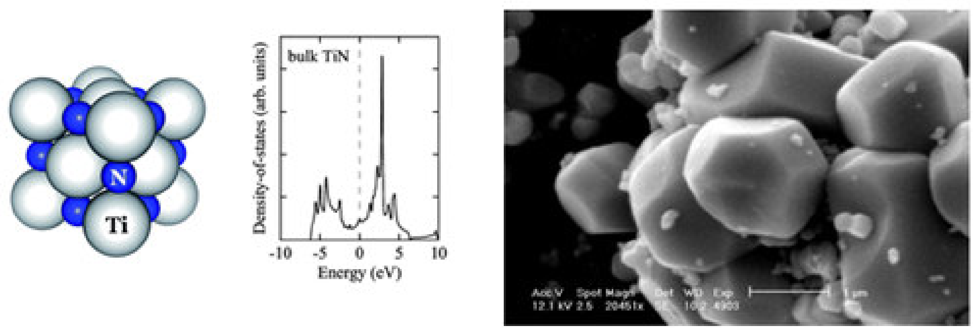

Figure 3: Morphology of TiN.

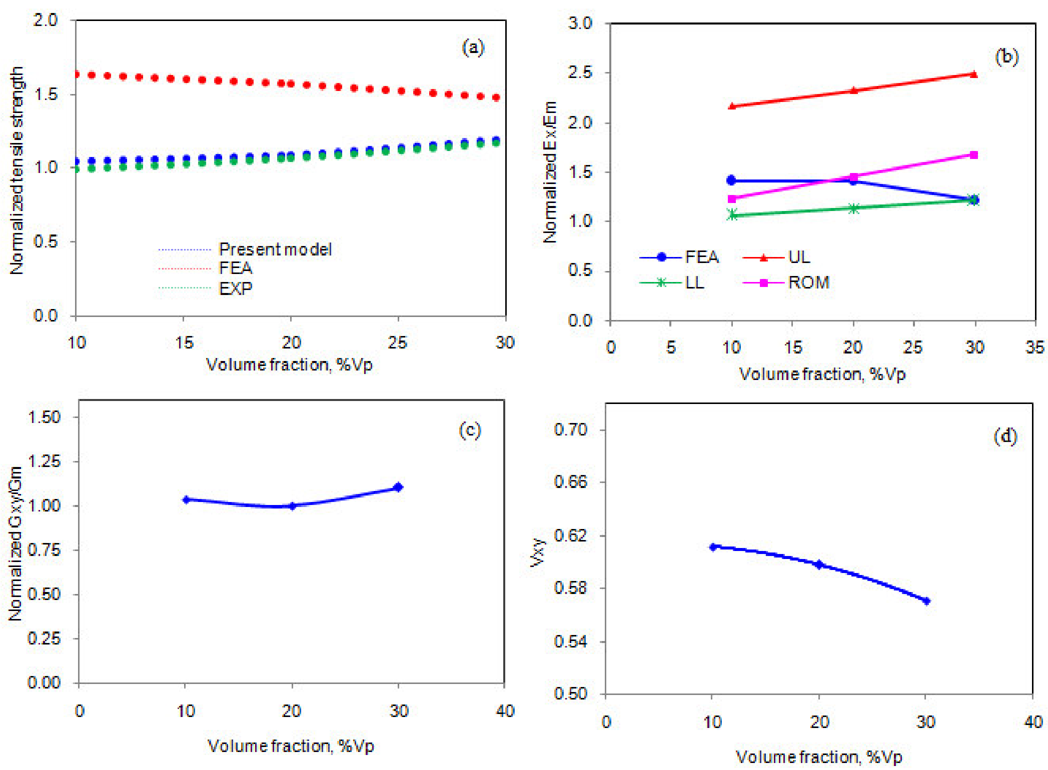

Figure 4: Effect of volume fraction on micromechanical behavior of AA8090/TiN composites.

4.1 Micromechanical Behavior

Figure 4a represents the normalized tensile strengths of the AA8090 alloy/TiN composites obtained by FEA, present mathematical model, and experimental test. The tensile strength is normalized with ultimate tensile strength of AA8090 alloy. The results obtained from present mathematical model and the experimental procedure are acceptable with a marginal difference. The stiffness of the composites increases with increase of volume fraction of TiN (figure 4b). The upper limit (UL) values computed by the present mathematical model are higher than those values obtained by the 'Role of Mixtures (ROM)'and FEA. This is because of assumption of porosity in the present mathematical model. The shear strength of the composites increases with increase in volume fraction of 20% TiN (figure 4c). The major Poisson's ratio decreases with increase of volume fraction of TiN particles (figure 4d).

4.2 Fracture Analysis

If the particle deforms in an elastic manner (according to Hooke's law) then,

$$\tau = \frac{n}{2}\sigma_p \tag{9}$$

where σ_p is the particle stress. If particle fracture occurs when the stress in the particle reaches its ultimate tensile strength, $\sigma_{p,uts}$, then setting the boundary condition at

$$\sigma_p = \sigma_{p,\,uts} \tag{10}$$

The relationship between the strength of the particle and the interfacial shear stress is such that if

$$\sigma_{P,uts} < \frac{2\tau}{n} \tag{11}$$

Then the particle will fracture. From the figure 5b, it is observed that the TiN nanoparticle was not fractured as the condition in Eq. (11) is not satisfied. For the interfacial debonding/yielding to occur, the interfacial shear stress reaches its shear strength:

$$\tau = \tau_{max} \tag{12}$$

For particle/matrix interfacial debonding can occur if the following condition is satisfied:

$$\tau_{max} < \frac{n\sigma_p}{2} \tag{13}$$

It is observed from figure 5a that the interfacial debonding occurs between TiN nanoparticle and AA8090 alloy matrix as the condition in Eq.(13) is satisfied.

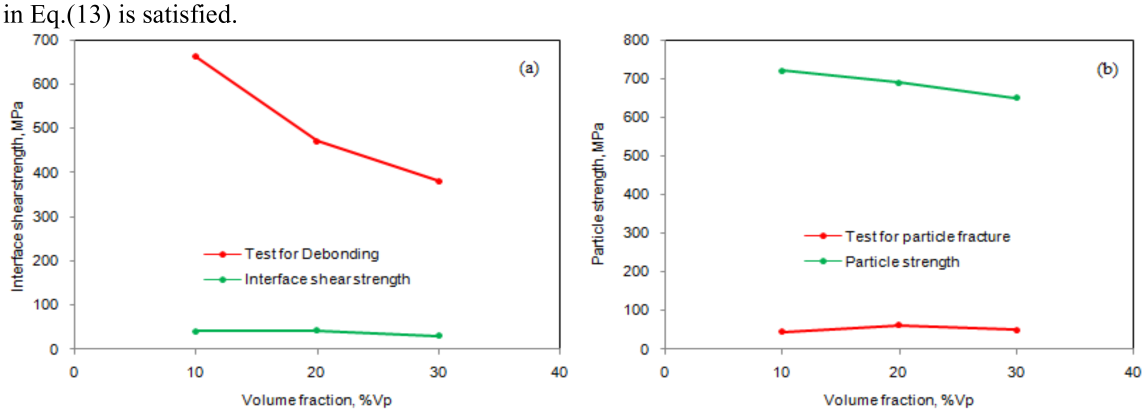

Figure 5: Criterion interfacial debonding (a) and for particle fracture (b).

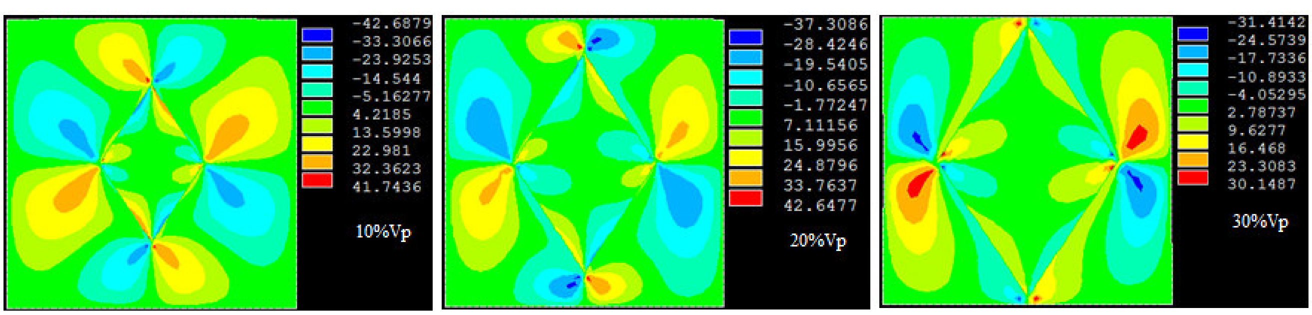

Figure 6: Images of tensile stress obtained from FEA.

The shear stresses induced at the interface are higher than those induced in the nanoparticle. Hence, the interfacial debonding was occurred between the particle and the matrix.

5. CONCLUSION

The shear stress is high at the interface leading to interfacial debonding in AA8090/TiN composites. The stiffness of the composite increases with increase of TiN reinforced particle in the matrix of AA8090 alloy.

REFERENCES

1. Voyiadjis, G.Z., Allen, D.H., 1996. Damage and interfacial debonding in compositesStudies in Applied Mechanics, vol. 44. Elsevier, Amsterdam.
2. Ho, S.Y., Fong, C.W., 1987. Correlation between fracture properties and dynamic mechanical relaxations in composite propellants. Polymer 28, 739–744.
3. B. Kotiveerachari, A. Chennakesava Reddy, Interfacial effect on the fracture mechanism in GFRP composites, CEMILAC Conference, Ministry of Defence, India, 20-21st August 1999.
4. A. Chennakesava Reddy, Assessment of Debonding and Particulate Fracture Occurrences in Circular Silicon Nitride Particulate/AA5050 Alloy Metal Matrix Composites , National Conference on Materials and Manufacturing Processes, Hyderabad, India, 27-28 February 1998, pp. 104-109.
5. A. Chennakesava Reddy, Evaluation of Debonding and Dislocation Occurrences in Rhombus Silicon Nitride Particulate/AA4015 Alloy Metal Matrix Composites, 1st National Conference on Modern Materials and Manufacturing , Pune, India, 19-20 December 1997, pp. 278-282.
6. S. Sundara Rajan, A. Chennakesava Reddy, Deformation Behavior of AA8090/ TiO_2 Nanoparticulate Reinforced Metal Matrix Composites with Debonding Interfaces, 2nd International Conference on Composite Materials and Characterization, Nagpur, India, 9-10 April 1999, pp. 245-248.
7. A. Chennakesava Reddy, Cohesive Zone Finite Element Analysis to Envisage Interface Debonding in AA7020/Titanium Oxide Nanoparticulate Metal Matrix Composites , 2nd International Conference on Composite Materials and Characterization, Nagpur, India, 9-10 April 1999, pp. 204-209.
8. A. Chennakesava Reddy, Micromechanical Modelling of Interfacial Debonding in AA1100/Graphite Nanoparticulate Reinforced Metal Matrix Composites, 2nd International Conference on Composite Materials and Characterization, Nagpur, India, 9-10 April 1999, pp. 249-253.
9. A. Chennakesava Reddy, Local Stress Differential for Particulate Fracture in AA2024/Titanium Carbide Nanoparticulate Metal Matrix Composites, National Conference on Materials and Manufacturing Processes, Hyderabad, India, 27-28 February 1998, pp. 127-131.
10. B. Kotiveera Chari, A. Chennakesava Reddy, Effect of Debonding on Overall Behavior of AA3003/Titanium Carbide Nanoparticulate Reinforced Metal Matrix Composites, 2nd International Conference on Composite Materials and Characterization, Nagpur, India, 9-10 April 1999, pp. 220-224.
11. H. B. Niranjan, A. Chennakesava Reddy, Effect of Particulate Debonding in AA5050/Boron Nitride Nanoparticulate Reinforced Metal Matrix Composites, 2nd International Conference on Composite Materials and Characterization, Nagpur, India, 9-10 April 1999, pp. 230-234.
12. P. M. Jebaraj, A. Chennakesava Reddy, Interface Debonding Prediction Technique for Tensile Loaded AA6061/Zirconium Oxide Nanoparticulate MMC, 2nd International Conference on Composite Materials and Characterization, Nagpur, India, 9-10 April 1999, pp. 235-239.
13. S. Sundara Rajan, A. Chennakesava Reddy, FEM Model for Volume Fraction Dependent Interface Debonding in TiN Nanoparticle Reinforced AA7020 Metal Matrix Composites, 2nd International Conference on Composite Materials and Characterization, Nagpur, India, 9-10 April 1999, pp. 240-244.
14. A. Chennakesava Reddy, Interfacial Debonding Analysis in Terms of Interfacial Tractions for Titanium Boride/AA3003 Alloy Metal Matrix Composites, 1st National Conference on Modern Materials and Manufacturing , Pune, India, 19-20 December 1997, pp. 124-127.
15. B. Kotiveera Chari, A. Chennakesava Reddy, Interfacial Debonding Analysis in Nanoparticulate Reinforced Metal Matrix Composites of AA8090/Zirconium Carbide, 2nd International Conference on Composite Materials and Characterization, Nagpur, India, 9-10 April 1999, pp. 210-214.
16. H. B. Niranjan, A. Chennakesava Reddy, Debonding Failure and Volume Fraction Effects in Nano-reinforced Composites of AA2024/Silicon Oxide, 2nd International Conference on Composite Materials and Characterization, Nagpur, India, 9-10 April 1999, pp. 215-219.
17. P. M. Jebaraj, A. Chennakesava Reddy, Analysis of Debonding along Interface of AA4015/Magnesium Oxide Nanoparticulate Reinforced Metal Matrix Composites, 2nd International Conference on Composite Materials and Characterization, Nagpur, India, 9-10 April 1999, pp. 225-229.